LIMNOLOGY
and
OCEANOGRAPHY: METHODS

Limnol. Oceanogr.: Methods 12, 2014, 390–406

Autonomous bed-sediment imaging-systems for revealing temporal variability of grain size

Daniel Buscombe[1], David M. Rubin[2], Jessica R. Lacy[2], Curt D. Storlazzi[2], Gerald Hatcher[2], Henry Chezar[2], Robert Wyland[2], and Christopher R. Sherwood[3]*

[1]United States Geological Survey, Flagstaff, Arizona, USA
[2]United States Geological Survey, Santa Cruz, California, USA
[3]United States Geological Survey, Woods Hole, Massachusetts, USA

Abstract

We describe a remotely operated video microscope system, designed to provide high-resolution images of seabed sediments. Two versions were developed, which differ in how they raise the camera from the seabed. The first used hydraulics and the second used the energy associated with wave orbital motion. Images were analyzed using automated frequency-domain methods, which following a rigorous partially supervised quality control procedure, yielded estimates to within 20% of the true size as determined by on-screen manual measurements of grains. Long-term grain-size variability at a sandy inner shelf site offshore of Santa Cruz, California, USA, was investigated using the hydraulic system. Eighteen months of high frequency (min to h), high-resolution (μm) images were collected, and grain size distributions compiled. The data constitutes the longest known high-frequency record of seabed-grain size at this sample frequency, at any location. Short-term grain-size variability of sand in an energetic surf zone at Praa Sands, Cornwall, UK was investigated using the 'wave-powered' system. The data are the first high-frequency record of grain size at a single location of a highly mobile and evolving bed in a natural surf zone. Using this technology, it is now possible to measure bed-sediment-grain size at a time-scale comparable with flow conditions. Results suggest models of sediment transport at sandy, wave-dominated, nearshore locations should allow for substantial changes in grain-size distribution over time-scales as short as a few hours.

Variation in nearshore bed-sediment grain size

Nearshore sediment transport determines the fate of seabed nutrients, contaminants, and pathogens; asserts control on the seabed and water column as habitats; and drives changes in seafloor topography which, in turn, affect wave transformation processes, spatial gradients in energy dissipation, and nearshore hydrodynamic circulation patterns. Relatively small changes in grain size have been shown to change the sign (depositional or erosional) of nearshore net sand transport rates (Ribberink and Chen 1993); affect the vertical grain-size distribution in suspension (McFetridge and Nielsen 1985); and the shape of suspended sediment concentration profiles (Conley et al. 2008). Laboratory experiments with graded beds simulating very high energy sheet-flow conditions show preferential transport of the coarse fractions in the mixture (e.g., van der Werf et al. 2006), and that the transport of each size-fraction is strongly influenced by the presence of other fractions (e.g., Wilcock 1988).

Model calculations of suspended-sediment flux have been shown to become highly inaccurate within hours if the effects of variable bed-sediment grain-size are ignored, because waves and currents can modify the spatial distribution of seabed sediments in a variety of shelf settings over this time-scale (Harris and Wiberg 2002). However, advances in modeling grain-size sorting (spatial segregation) and its underlying selective transport mechanisms are hampered by few observations at sufficient coverage/frequency with which to compare theory. The result is that most nearshore (e.g., Bailard 1981; Larson and Kraus 1995) and regional shelf (e.g., Harris and Coleman 1998; Zhang et al. 1999; Cookman and Flemings 2001) models tend to oversimplify grain-size distribution effects on sediment transport because detailed observations of the behavior of a mixture of size fractions is lacking.

A more complete understanding of the role of grain size in the physics of sediment transport requires the collection of grain-size data with more temporal and spatial coverage, and

*Corresponding author: E-mail: dbuscombe@usgs.gov

Acknowledgments

Full text appears at the end of the article.

DOI 10.4319/lom.2014.12.390

higher resolution with less uncertainty. Presently, such measurements (e.g., Miller and Ziegler 1958; Greenwood and Davidson-Arnott 1972; Masselink et al. 2008; Austin and Buscombe 2008) are rare, sporadic in location, biased to shallow water, and short-lived (a few hours to a few weeks). The lack of such measurements to date is primarily because of a technical and logistical shortfall, rather than a perceived lack of importance.

A huge discrepancy remains between our ability to measure water-column properties (flow and suspended sediment), and our ability to measure bed-sediment characteristics (Wheatcroft et al. 2007), including grain size, concentration, shape, permeability, and packing. Improved understanding of processes dependent on the dynamic behavior of these seabed characteristics requires measurements at much higher frequency than has previously been possible, which in turn, necessitates advances in directly measuring these seabed properties at sufficient resolution.

Recently, high-resolution (order μm) grain-size measurements have been made possible using submersible bed-sediment camera microscope systems (Rubin et al. 2007) and automated analysis techniques (Rubin 2004; Buscombe 2008; Buscombe et al. 2010; Buscombe and Rubin 2012; Buscombe 2013), which provide highly accurate (within 20% r.m.s. error: Warrick et al. 2009; Buscombe et al. 2010; Buscombe and Rubin 2012; Buscombe 2013) estimates of grain size. This approach has the potential to offer unparalleled spatial or temporal resolution using relatively simple, completely automated analysis procedures.

Scope and objectives

Several processes might cause grain size to change at a point on the seabed, but only some are directly due to instantaneous waves and currents (Table 1). Each of these processes has a characteristic time and spatial scale (Fig. 1). To cover the required range of time-scales, measured seabed grain-size time-series ideally need to be long (months to years), and sampled frequently (minutes to hours). Having identified this need, the objectives of this study were as follows: (1) To detail a novel instrument designed to obtain, in an automated fashion, images of a sandy seabed at a frequency of minutes to hours, a timescale comparable to changes in flow; (2) to use and evaluate published techniques to acquire grain-size estimates from these images; (3) to build an almost 18-month single-point time-series of accurate grain-size data in this way; (4) to assess the time-scales at which an equivalent grain-size variability might be expected over space, by evaluating the variability of grain size at one point compared with both the immediate vicinity and the entire nearshore.

In these Eulerian observations, changes in grain size may or may not be directly associated with waves and currents, but may instead be caused by indirect mechanisms (Fig. 1 and associated Table 1). Those grain-size changes that are associated with instantaneous hydrodynamics require differential transport of different sizes. Over short (time- and spatial-) scales (up to days, and over tens of meters) this is assumed to occur principally due to resuspension by waves removing (or adding) the 'mobile fraction' from the population (e.g., Harris and Wiberg 2002). The sediment composition of the bed might be altered by advection of sediment into and out of the area by currents, over scales up to or greater than tens of meters, perhaps depending on the time scale. Table 1 reveals that, due to a broad range of time and length scales that co-occur, the sampling frequency should be designed to capture the scales/processes of interest. Trends and variability in the statistics of the grain size distribution at a point over time, if sampled at sufficiently high frequency for a sufficient length of time, should therefore characterize sediment transport processes integrated over a scale of tens of meters. This new measurement technology should reveal the required time scale and degree of variability.

Materials and procedures

The hydraulic underwater video microscope system

The system consisted of a remotely operated underwater video microscope, cabled to a computer located at the end of Santa Cruz Municipal Wharf (Fig. 2). The system (Fig. 3) was designed to collect high-frequency, very high-resolution (3.65 μm/pixel) microscopic images of the seabed, and consisted of a video camera fitted with macro lens inside an underwater housing. Images were used to measure bed-sediment grain size. Hydraulically controlled, it essentially had just two movable parts and the simplicity of its design allowed it to function in the ocean environment for several months at a time without maintenance or repair. An additional tripod was positioned 8 m away in the same water depth of 10 m (Fig. 2), equipped with acoustic instruments for measuring bed-form dimensions (sector-scanning and pencil-beam sonar); an Acoustic Doppler Velocimeter (ADV), Pulse-Coherent Acoustic Doppler Velocimeter (PCADP) and Acoustic Doppler Current Profiler (ADCP) for measuring tides, waves, and currents; as well as a Laser In-Situ Scattering Transmissometer (LISST) and Optical Backscatter Sensor (OBS) for suspended-sediment concentrations (Lacy et al. 2012).

The system was deployed in October 2008 and recovered 18 months later in March 2010. The study site was outside the zone of wave breaking, even during storms. Scuba diver support ensured that instrument failures and fouling were remedied without recovering the system. The tripod remained stationary while divers periodically cleaned the instruments in situ, and swapped instruments when necessary. As to be expected from testing phases of a new instrument, there were periods of system downtime. The first, between 22 Dec 2008 and 27 Jan 2009, was caused by a failure of the hydraulic system due to a leaking stainless steel cable fitting. A part of the quick-release fitting was not stainless steel and had rusted. The fitting was replaced after a diver identified the problem, and it took a few weeks to find a solution for how to carry out the repair underwater. A hiatus in August and September 2009 was

Table 1. Hypothesized processes, and associated time scales, which can cause grain size to vary at a single point on the continental shelf.

Process	Time scale of grain-size variability	Spatial scale of grain size decorrelation	Relation of grain size changes to waves and currents
(1) Local surface patchiness on a scale of camera re-positioning (up to few cm).	Varies at a single instant in time.	Observations up to a few cm apart are uncorrelated.	Not related to waves or currents; no sediment transport required.
(2) Local surface patchiness. Grain size can vary at a point as organized grain segregations pass by.	The time for a whole patch to pass by the measurement location. Hours to days.	The size of a homogeneous patch of grain size, up to tens of m.	Sediment transport required, but changes in grain size unrelated to instantaneous waves or currents.
(3) Bedform trough / crest differences. Grain size at 2 nearby locations might be positively or negatively correlated, depending on the phase between topography at those 2 locations.	Varies quasi-periodically as ripple troughs and crests pass by (e.g. Doucette, 2002). Hours to weeks.	The distance between troughs and crests (cm to m).	Frequency of grain-size changes related to waves and/or currents if they control the bedform migration period, but particular instances when sediment is coarse and fine are unrelated to waves or currents.
(4) Change in bedform size alters depth of scour, exposing or incorporating substrate with different grain size.	Bedforms change rapidly when a storm starts and return more slowly to pre-storm state (e.g. Hay and Wilson, 1994). Hours to days, but may be months between storms.	Bedforms grow and decay *in situ* (cm to m). Observations separated by several m are uncorrelated.	Changing wave conditions make larger bedforms that scour in troughs down into substrate with different grain size.
(5) Stratification caused by passage of train of ripples (e.g. Scheidegger and Potter, 1967).	Varies quasi-periodically as ripple train passes by. Hours to weeks.	The length of the ripple train (m to tens of m).	Ripples sort the grains leaving a coarse, less active lag at an elevation near the deeper troughs, and fine active sand near surface.
(6) Selective re-suspension without advection.	Individual waves, wave groups, or storms (e.g. Harris and Wiberg, 2002). Hours to days.	Scale beyond which there is non-uniform orbital velocity and grain size.	Bed coarsens when fine sediment is preferentially resuspended, and bed fines when sediment settles out. Grain size decreases if fine sediments settle and remain at surface. If that fine sediment mixes with subsurface, no net grain size change over the event.
(7) Sediment advection in the presence of a large-scale spatial gradient in grain size	Wave groups or storms over hours to days. Large scale gradient in grain size develops over up to tens of years.	Tens of m to several km.	Winnowing or introduction of fines, depending on direction of advection relative to the spatial gradient.
(8) Onshore / offshore transfer of sediment.	Days to years (e.g. Shepard, 1950).	Up to several km.	Change occurs during storms or reverses between storms.

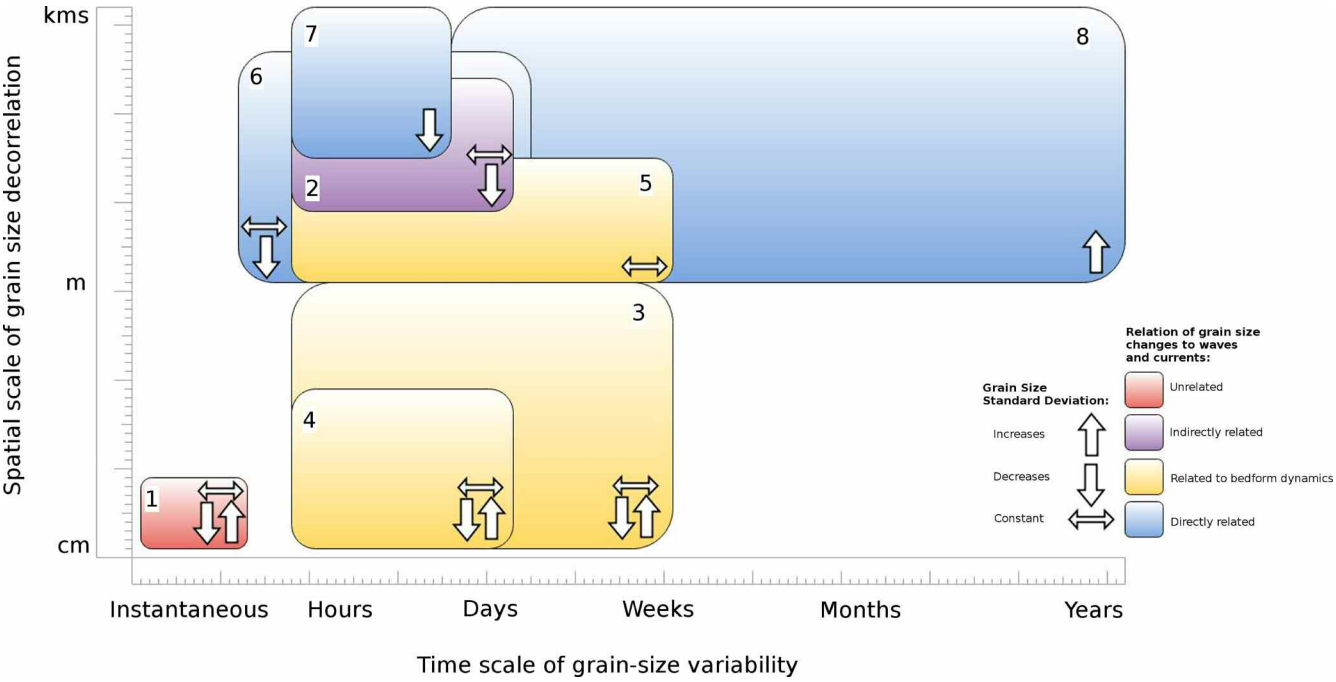

Fig. 1. Graphic showing the likely time and spatial scales of the processes described in Table 1, which might cause grain size to vary at a point on the continental shelf. The numbers in the boxes correspond to the rows in Table 1. The spatial scale of grain size decorrelation is the distance over which the autocorrelation in grain size becomes insignificant.

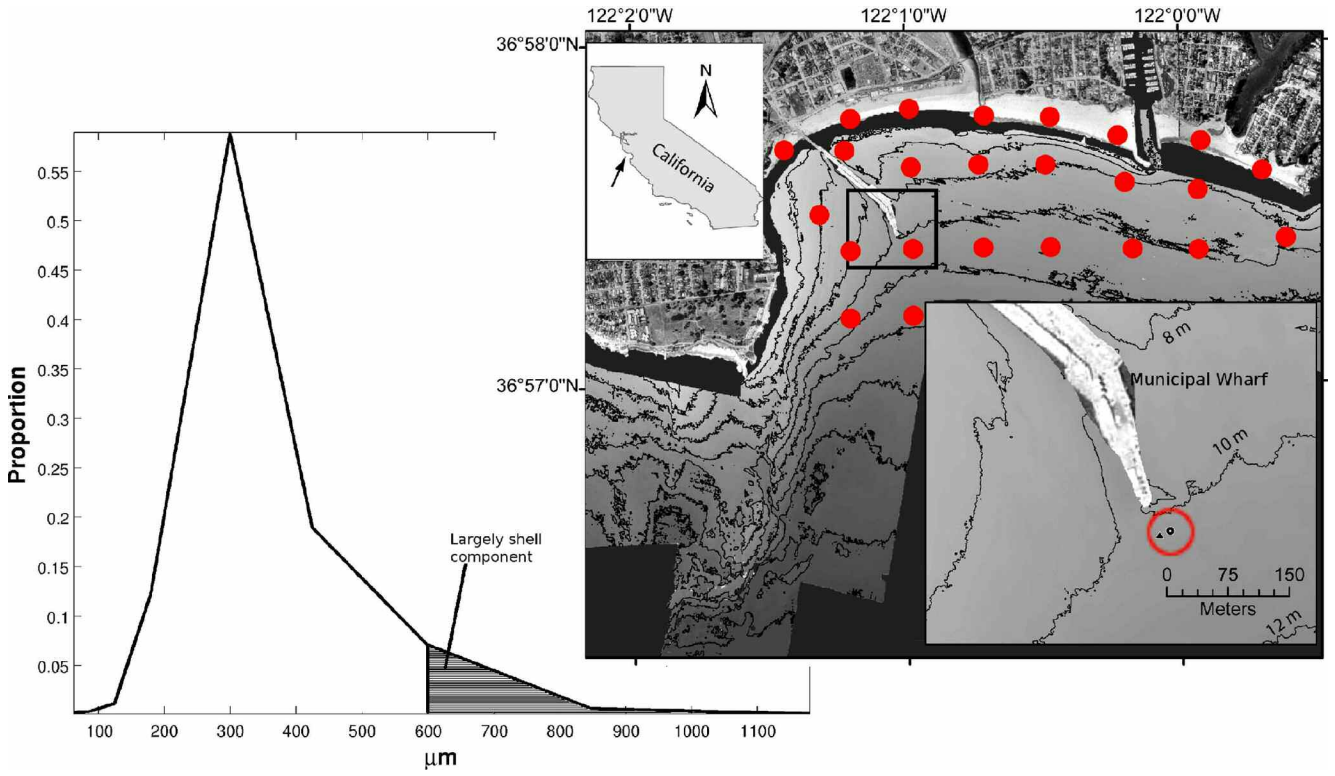

Fig. 2. Santa Cruz, northern Monterey Bay, central California. Hydraulic camera system and main instrument tripod positions marked by the circle and triangle, respectively, in the map inset. The inset map shows the extent of diver grain size surveys, as a circle around the immediate vicinity of the tripod. The larger map shows regular sampling locations for grain size in the winter of 2009-2010. Bottom-left panel: bulk seabed grain-size distribution for this site, obtained from sieving grab samples taken in the autumn of 2008 and spring of 2009.

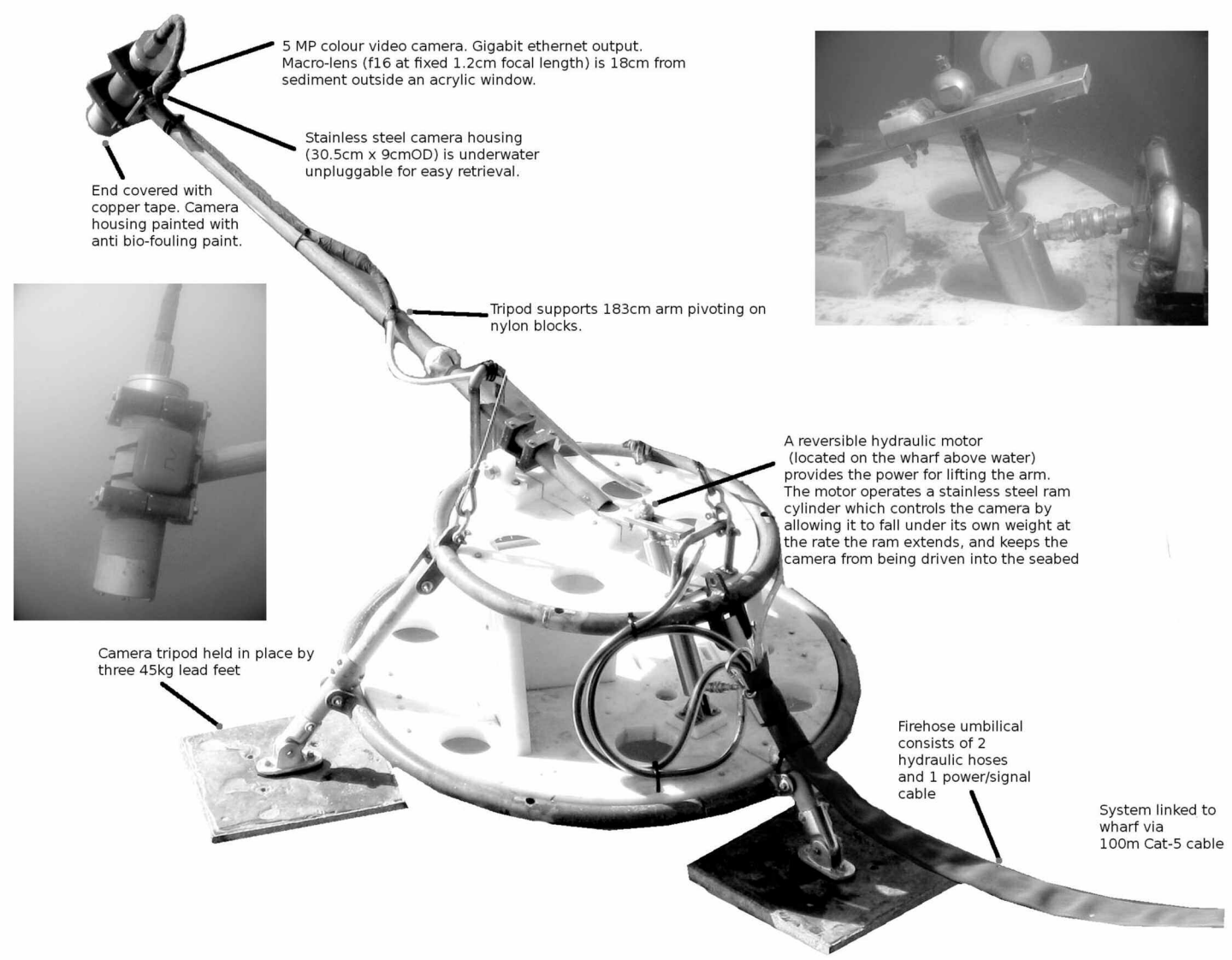

Fig. 3. Camera motion and image capture were controlled from the acquisition computer located on the Santa Cruz Wharf, via a dedicated Ethernet network connection. A set of internet-accessible time standard providers were used to maintain robust time synchronization between the images and all other data collected by the seafloor observatory. A computer controlled the hydraulic motor, which lowered the camera to the seabed. The motor was located on the wharf, which made it easy to service, add bio-degradable hydraulic fluid if needed, and even replace if required.

the result of biological fouling of the camera faceplate. The camera was recovered and the faceplate replaced. We believe it took so long for the camera to foul because of its frequent motion and contact with the seabed. The last downtime, in the last 2 weeks of November 2009, was caused by fouled cable connections. Unfortunately, despite the use of anti-fouling measures (such as copper tape, screens, and sensor guards) biological fouling is somewhat inevitable, therefore system maintenance by divers would have to be carried out periodically for a long-term system deployment.

The housing was lowered to the seabed at regular intervals to take an image. Once the image was acquired, the camera was powered down and the hydraulic pump was turned on in the reverse direction to lift the camera over 1.5 m from the seafloor. This minimized interference (drag and scour) with the bed. The hydraulic pump was run long enough to ensure the camera was completely lifted away from the seafloor and then powered down to wait for the next cycle. In the first few months between system deployment and 6 Feb 2009, the system acquired an image every 2 h. Between 6 Feb 2009 and 6 Mar 2010, when the system was finally recovered, this routine sample frequency was increased to once per hour.

Due to the potential for sediment disturbance by the camera, and sediment transport in front of the camera lens, the

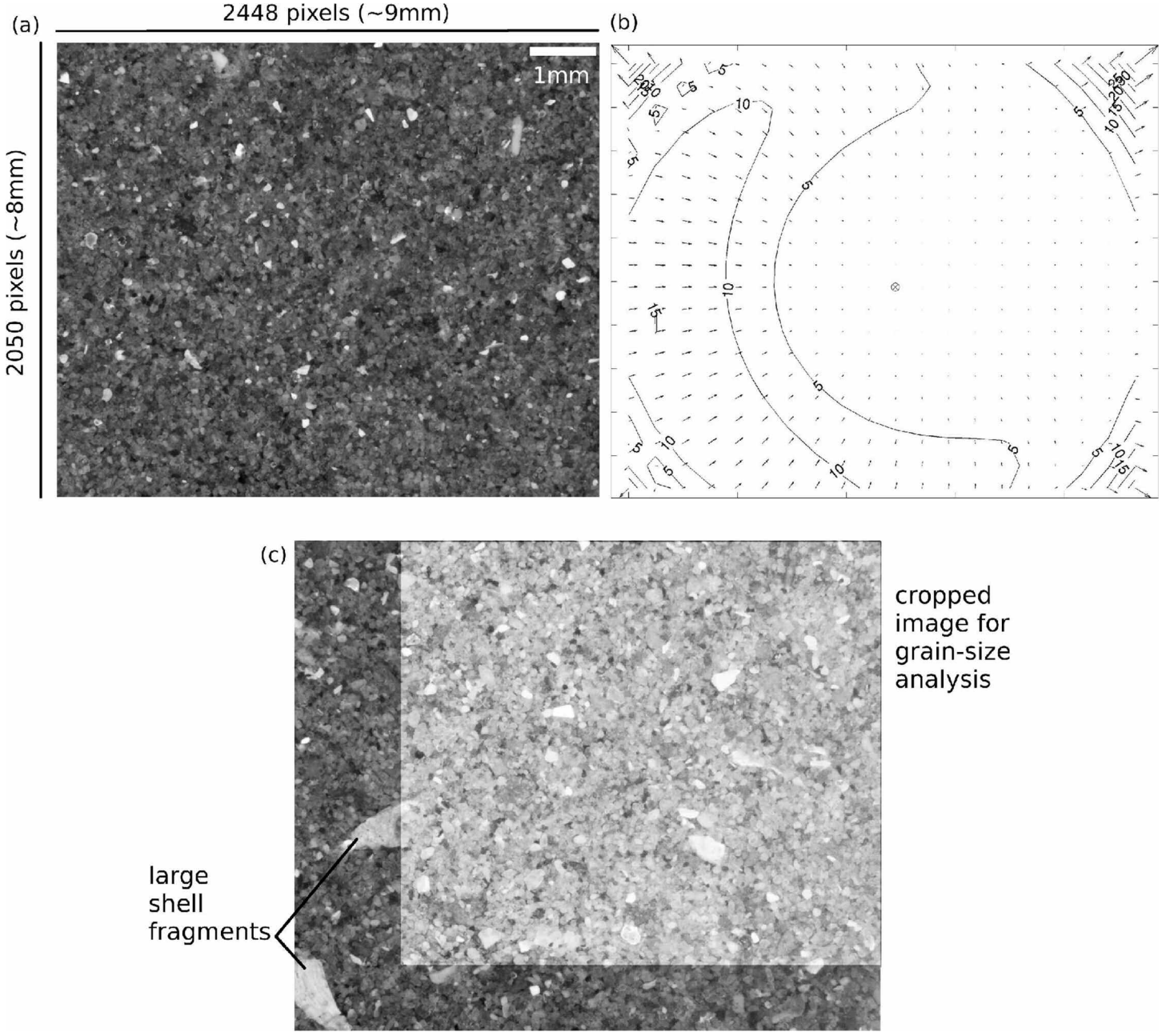

Fig. 4. (a) Typical sediment image with dimensions (resolution 3.65 microns/pixel, 1 mm white bar for scale); (b) camera distortion model (distortions in pixels; central marker is the camera's principal point) obtained through converging-line geometric correction (Hartley and Zisserman 2003) using a grid held in front of the camera; and (c) large shells removed by cropping to an image area ≥ 2/3 the original area.

camera lowered and rested on the sediment surface for a prescribed amount of time before the image was taken. This was initially set to 30 s, but due to concerns over the amount of drag around the camera at the bed surface, after 3 weeks (21 Nov 2008) the duration was reduced to 10 s. Repeated diver observations confirmed that this 10-s resting period did not cause scouring or enhanced resuspension. Image collection was automated, and images were automatically copied from the acquisition computer to a server via the internet twice a day.

The faceplate of the camera housing made contact with the seabed, with LED lights inside the housing to illuminate the bed. A diffuser was used to soften and uniformly spread the light. To minimize internal reflections of light, the interior of the housing in proximity to the lights was painted black. The system was carefully designed to ensure that every high-resolution (2448 × 2050 pixel) image was in focus with grains easily resolved by eye (Fig. 4a). A complete (radial plus tangential) intrinsic camera calibration (Hartley and Zisserman 2003;

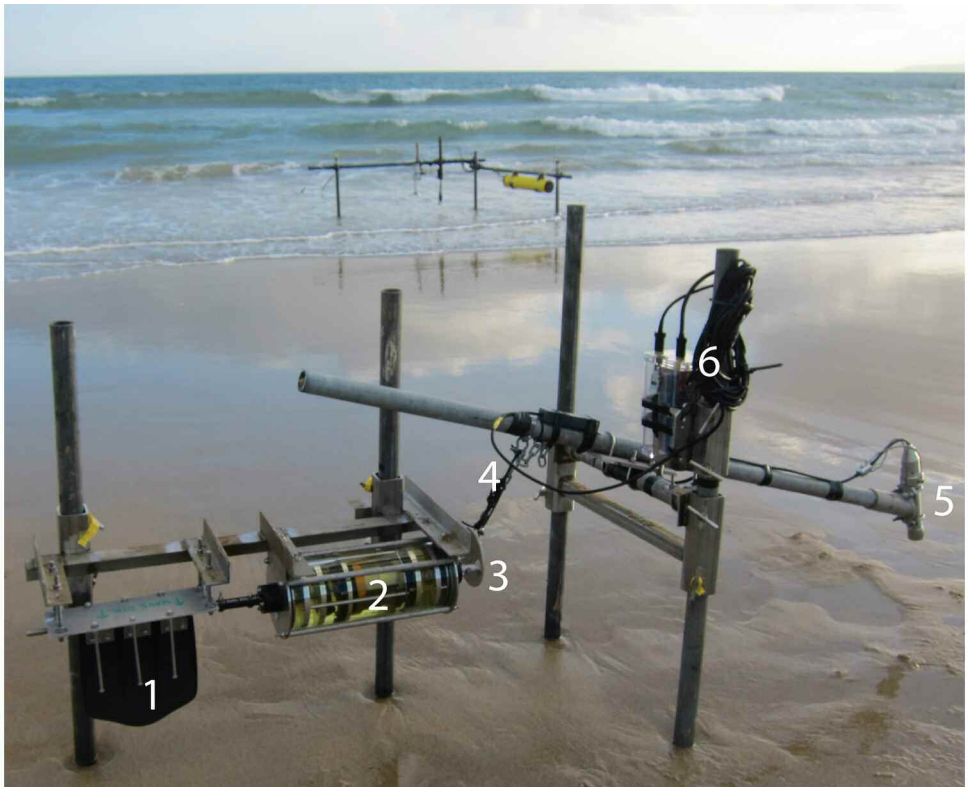

Fig. 5. 'Wave-powered' camera system. A paddle constructed from a dive fin (1) is pushed back and forth by waves, turning a ratcheting speed-reducer in an oil-filled cylinder (2). The rotating output wheel of the speed-reducer (3) pulls down on the chain (4), which raises the video camera (5). The time required to raise the camera from the bed to the top position depends on wave period, wave height, and water depth, but is typically a few tens of minutes. When the chain on the wheel (3) passes its lowest position, the ratchet allows the camera to fall to the bed, and a tilt sensor turns on a battery-powered video camera (5) and solid-state recorder (6) to collect a short sequence of video images (Fig. 6).

Heikkilä and Silvén 2007), implemented using OpenCV (2014) open-source computer vision software, revealed lens distortion (Fig. 4b). Each arrow in Fig. 4b represents the effective displacement of a pixel induced by the lens distortion. Notice that points at the corners of the image are displaced by as much as 20 pixels (73 μm) but most of the image is displaced up to 15 pixels (0–55 μm). This distortion is removed which and thus did not affect the grain-size results. This process involves remapping the image onto an undistorted plane using the intrinsic camera calibration parameters. The technical details of this process is well beyond the scope of the present manuscript, we therefore refer the reader to the open-source software used (OpenCV 2014), which have excellent technical descriptions. Further details and recommendations about macro-photography of sediment in natural environments may be found in Rubin et al. (2007) and Buscombe et al. (2010).

The 'wave-powered' system

Another system was developed for capturing bed sediment imagery in an energetic surf zone. It was termed the 'wave-powered' system because it used wave action to raise the arm to which the camera was attached above the bed to prevent bed scour. The system, shown and described in Fig. 5, was deployed at Praa Sands, a macrotidal coarse sand beach in Cornwall, UK, in May 2011. This system, not reliant on hydraulic lines for lifting the camera from the bed, can be rapidly deployed with no infrastructure and minimal logistics. The images (Fig. 6) obtained were analyzed for grain size and are being used to help understand selective resuspension processes in an energetic surf zone over short (hourly) timescales. The sample interval is irregular and dependent on wave orbital velocity. This typically increases in shallow water, or with larger wave heights and periods, which has the advantage that sampling is biased to more energetic conditions, which is also when bed sediment grain size might be changing at a faster rate. The disadvantage of such an irregular time series is that statistical analyses become more cumbersome.

Image quality control and pre-processing

To obtain highly accurate estimates of grain size, images underwent a rigorous semiquantitative quality control procedure that removed shell fragments, fecal pellets, and other organic material. Each image was viewed, and if necessary, cropped to provide the largest possible area containing only inorganic sediment grains. Buscombe et al. (2010) determined that grain-size estimates are accurate if the sediment image is at least the area of 1000 grains the size of the 25th percentile. For the Santa Cruz site, a rule of thumb for the minimum

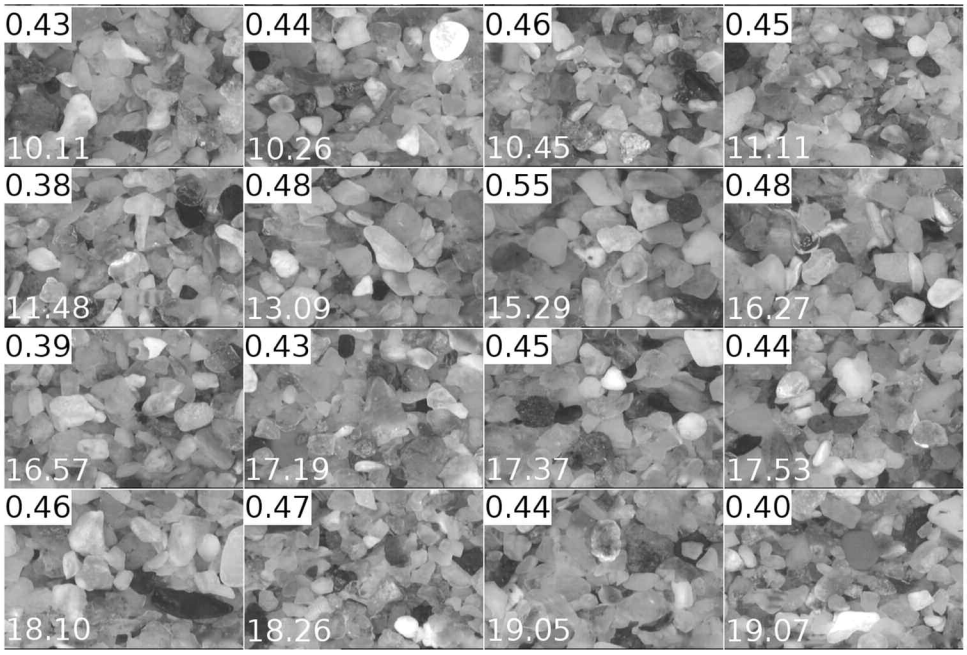

Fig. 6. Example time-series of images collected over 1 tide by the wave-powered system at Praa Sands, UK. The number in the bottom left corner is the time (24 h format) of the sample. The number in the top left corner is the calculated mean grain size in millimeters.

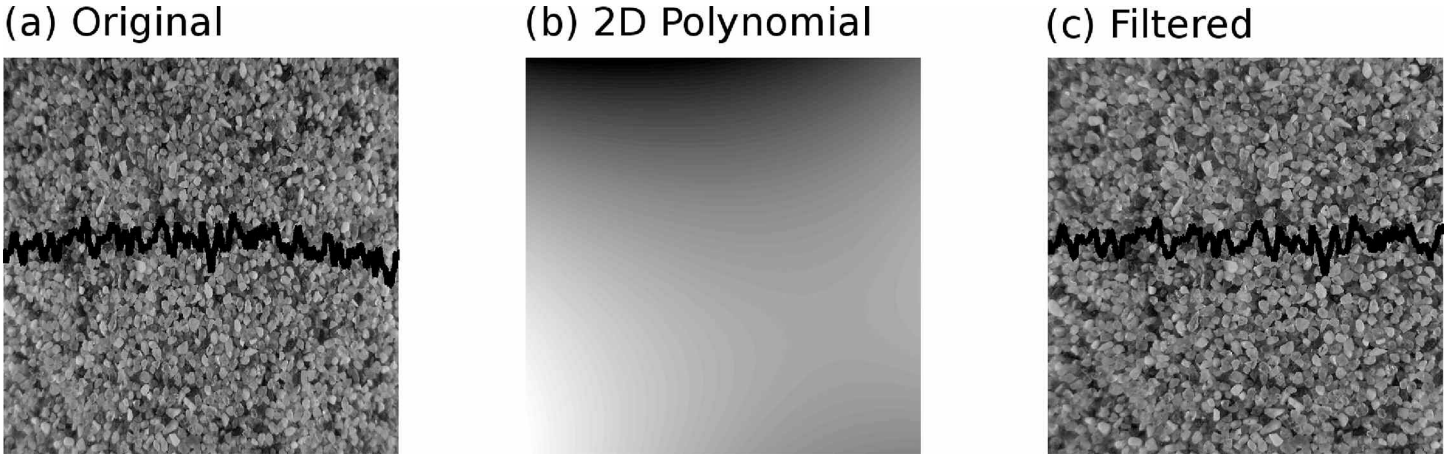

Fig. 7. Example filtering procedure to remove long-wavelength variations in image intensity. The original image (a) contains irregular lighting, which produces dips at the edges of the column-average intensity (black line). The linear 2D polynomial surface is constructed (b) and subtracted from the image. The filtered image (c) has a column-average intensity (black line) with no trend.

image area is that with a minimum dimension of at least 1800 pixels (≈2/3 original image dimension), based on a maximum 25th percentile grain diameter of 200 μm (Fig. 4c). When cropping, preserving the aspect ratio of the image is not necessary. This quality control procedure removed around 5% of the images, the majority of which were due to nongranular objects occupying too large an area of the image, or situated centrally such that the image could not be cropped according to the criteria outlined above.

Images were then filtered to remove large variations in intensity, which can introduce a coarse-bias to grain-size results. Nonuniform lighting, or most likely, incomplete contact of the camera faceplate with the sediment surface (for example, if well-developed ripples are present), produced shading variations much greater in wavelength than any grain scale. A simple two-dimensional linear polynomial ('trend surface') was calculated and removed from each image, which proved effective (Fig. 7).

Grain size

A total of almost 9000 images of the seabed, obtained using the hydraulic system in Santa Cruz, passed the quality control procedure, which prompted the need for a completely auto-

mated and robust method for estimating sediment-grain size. The method of Buscombe (2013) was used to provide estimates of the distribution of grain sizes. The grain-size distribution obtained is of all visible intermediate (b-axis) grain diameters present in the image. A grain size distribution is estimated from each image. This is estimated directly from each image by uncovering the typical length scales of the particles from the image's global wavelet spectrum. As such, neither tunable parameters nor calibration are required, nor is isolating the boundaries of every grain and measuring their properties. This method is the latest in a series of methods (Buscombe 2008; Buscombe and Masselink 2009; Buscombe et al. 2010; Buscombe and Rubin 2012) that follow from Rubin's (2004) observation that images of coarser grains successive pixels are more highly correlated than in images of finer grains. These methods have proved to be successful in a number of sedimentary environments, with a typical error of less than 20% (Rubin et al. 2007; Barnard et al. 2007; Warrick et al. 2009; Buscombe 2013).

The method of Buscombe (2013) estimates the grain size distribution using spectral analysis on the entire image, by means of the global wavelet power spectrum that quantifies the variance contributions of grain-scale wavelengths within the image. The global wavelet power spectrum is calculated by aggregating the wavelet power spectra from the pixel intensities in every row of the image. The wavelet technique was found to be less sensitive than previous Fourier-based methods (Buscombe et al. 2010; Buscombe and Rubin 2012) to noise and small sample sizes (small fields of view and/or small numbers of relatively large grains), providing that the pixel intensities across individual grains are more slowly varying and larger in value (brighter) than the abrupt intensity differences between grains, in darker interstices. The technique has been tested on hundreds of sampled images from a wide range of sedimentary environments Buscombe (2013). However, to test the technique for use with the (hydraulic) camera system specifically, grain diameters in 34 images were manually identified and measured. The images were drawn at random from a catalogue of images stretching over several months. The 'point-counting' method of Barnard et al. (2007) was employed whereby, in each digital image, a grid composed of a number of intersections was drawn and the intermediate (b-axis) diameter of the grain, measured as the center-to-center distance between interstices, underneath each grid intersection measured. This procedure makes grain selection free from operator bias (Warrick et al. 2009). Grain sizes as estimated using the automated techniques were within 20% (root-mean-squared error) of those determined by point counts (Fig. 8).

The standard deviation of the measurements of mean grain size is 100 μm (for data collected over a given week, to avoid real changes in grain size). Standard error of the mean reduces by the square root of the number of measurements (corresponding to ±30 μm for 10 measurements). In the present study, a running mean of 6 hourly samples would have an estimated measurement error of less than 10% due to convergence on the mean. One potential source of error is the presence of very fine sediment particles. Buscombe et al. (2010) found the lower limit of a resolvable grain size to be 3 times the spatial (pixel) resolution, which for the present system is ≈10 μm. Smaller grains will be under-resolved, and if arranged in clusters, will be interpreted by the grain-size-analysis algorithm as larger particles. Grab samples show that, at this site, such size fractions constituted < 10% by weight (bulk grain-size distribution inset in Fig. 2). Although no cores were avail-

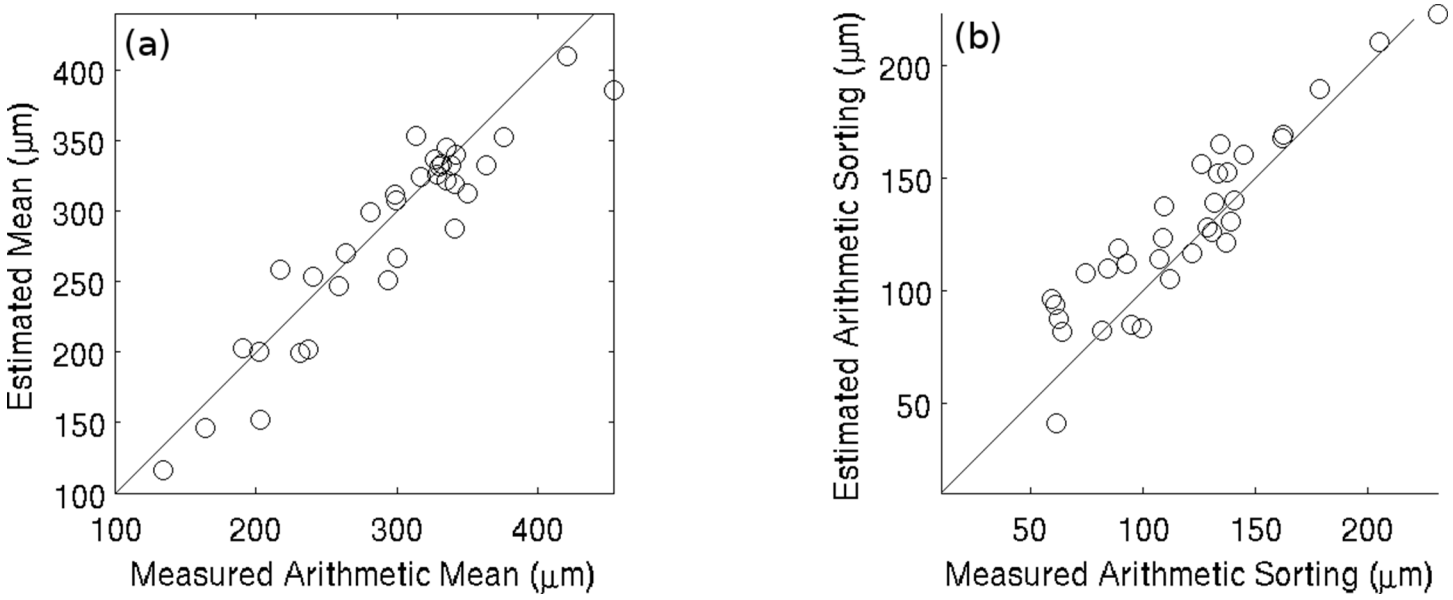

Fig. 8. Comparison between grain size (a) mean and (b) standard deviation manually measured by point counts on sample images and estimates from the automated statistical grain-size-analysis methods.

able to determine whether muds accumulated in surface veneers, scrutiny of the images strongly suggested otherwise: that patches of these fine particles were rarely, if ever, in evidence at the surface presumably because of a lack of fine sediment supplies during the study period and the energetic wave-dominated environment. Unresolvable (sub-pixel) fine particles within the interstices of larger, resolvable, particles would create a spurious coarse bias in the grain-size distribution estimate, which would have to be corrected empirically. Because area occupied by a sand grain in images is proportional to its squared diameter (Diplas and Fripp 1992), it was decided to ignore this small but unquantified error. However, this serves to highlight the importance of cropping out large (generally non-sand) grains, such as shell fragments, with disproportionately large areal coverage relative to their volumetric abundance. Fines, shells, and bioturbation marks were not a significant issue at the present site, but may pose more of a problem in images of the seabed in deeper water.

One advantage of the present technique measures the grain size only of the surface grains, which are interacting with the flow. The frequency of measurements, and the ability to reliably extract an estimate of grain size distribution from each image (without aggregating several images), is sufficient to capture the evolution of the bed grain size distribution as a result of erosional and depositional processes.

Representativeness of sampling frequency and sample location

To assess whether the normal operational sample frequency of once per hour was sufficient to capture the variability in grain size, the seabed was imaged at the highest practical frequency (once every 10 minutes; limited only by the speed of the hydraulic cycle), and the statistics of the high-frequency records were compared with the same records down-sampled to once per hour.

The spatial representativeness of the sample location was assessed using images from photographic surveys carried out by scuba divers, conducted on 10 April (following a period of moderate energy wave activity) and 29 July 2009 (after a period of very calm waves followed by a minor storm event). On each occasion, divers used a hand-held underwater camera to image the seabed at prescribed points measured with a tape near the camera system tripod, between 1 m and 20 m distance in each of the 4 compass directions (Fig. 2). The hand-held camera was fitted with a macro-lens in a waterproof housing (a design similar to that shown in Figs. 2 and 4 of Rubin et al. [2007]). The camera was calibrated for geometric distortion, and grain size was obtained using the same method as for the images acquired using the hydraulic system.

Regional grain size data

As well as the grain size data at a single location provided by the hydraulic system in Santa Cruz, regional grain size data collected during the autumn and winter 2009-2010 are also available. Grain size surveys were carried out (Fig. 2) using a boat-deployed camera identical to that inside the hydraulic system (Storlazzi et al. 2010), and images from the surveys were analyzed for mean grain size in the same way.

Assessment

Representativeness of sampling frequency and sample location

The analysis detailed in the above section was carried out to assess the temporal representativeness of the location of the hydraulic system. On the first occasion, the 10-min record mean and standard deviation were 302 and 21 μm (Fig. 9). The same record sub-sampled at every 60 min (the usual sampling frequency) had mean and standard deviation of 304 and 25 μm, respectively. On the second occasion, the 10-min mean and standard deviation were 287 and 19 μm, respectively. The same record sub-sampled to every 60 min had a mean and standard deviation of 289 and 12 μm. This result suggests that very short-lived changes in grain size not captured by an hourly sampling scheme are not considered significant for sediment transport because they do not significantly affect the mean or standard deviation.

Grain size within tens of meters of the hydraulic system location was always within 50%, and more typically within 30%, of the measurement taken nearest in time (Fig. 10). This is broadly in line with typical weekly variability, calculated from the entire record, and gives a reasonably good indication that the location of the hydraulic system was obtaining images that were on, at least, the two time periods of the respective surveys, representative of the surrounding area, and included the immediate vicinity of the instrument tripod. This spatial variability suggests that to adequately represent the time-series of grain size dynamics of the measurement location and its immediate vicinity, hourly grain-size measurements should be time-averaged to remove the variability associated with local patchiness in grain-size advected past the measurement location (Table 1). Grain-size estimates from hourly sampling would be adequate to identify patch of homogeneous (organized) sediment, or sorted bedforms (Table 1), as it advects past the measurement location, providing the advection rate is steady, and other resuspension processes are not occurring simultaneously.

Time-series

Significant wave height (H_s), representative bottom-orbital velocity (u_b), peak wave period (T_p) (Fig. 11), and wave direction were calculated from the semi-hourly 4-Hz velocity and pressure data collected by the ADV using the spectral methods of Madsen (1994). When ADV data were not available, 1-Hz data from the PCADP were used. Summary statistics of hydrodynamic parameters are provided in Table 2.

The site was typified by narrow-banded (8-16 s; Fig. 11b) waves with a very narrow directional spread (160-190° N). Wave heights (H_s) were generally modest, typically around 0.5 m (Fig. 11a), which generated u_b of 0-0.8 m s^{-1} (Fig. 11c). Waves with $H_s > 1$ m constituted 5.3% of the total record. The winter of 2009-2010 (mean $H_s = 0.6$ m) was considerably (50%) more

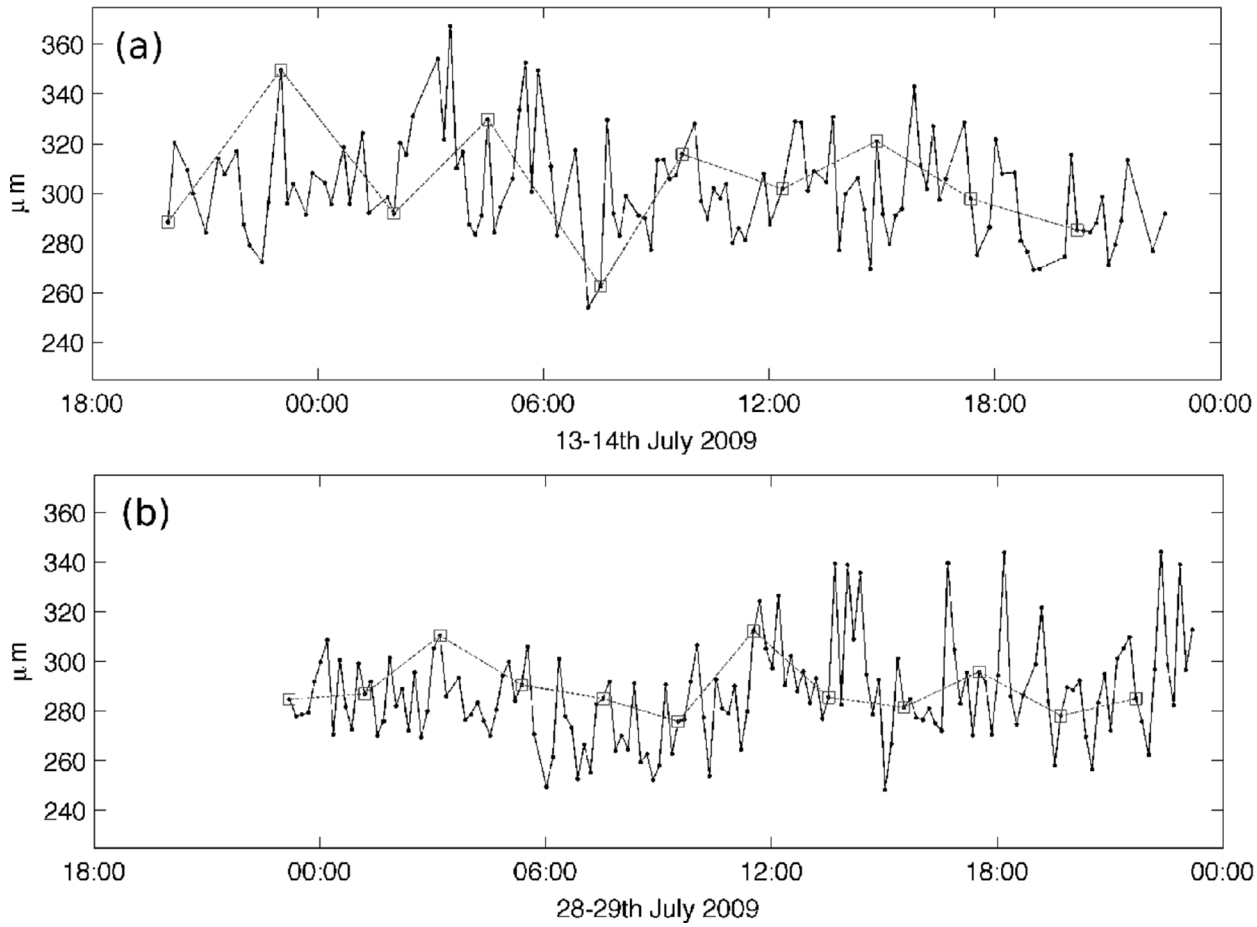

Fig. 9. Mean grain size from two occasions at a very high frequency (10-min) sampling rates. In these, the dashed line connecting the squares are the data sampled at the normal-operation hourly sampling rate.

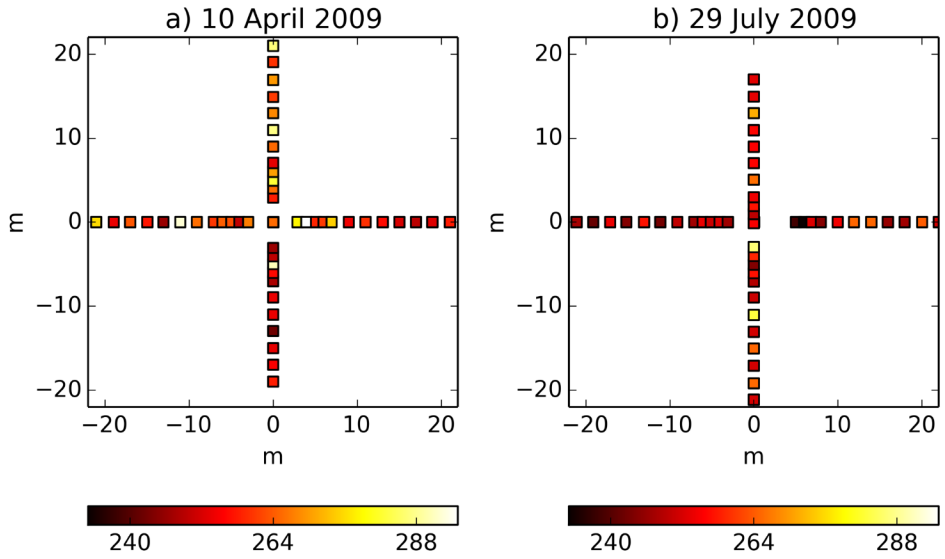

Fig. 10. Spatial variability of grain size around the sampling location of the hydraulic system, from two dives on the dates shown. Grain size from North-South and East-West transects, in meters from the hydraulic instrument location at (0,0), are expressed in μm. The diver surveys, although necessarily carried out in calm conditions, followed periods of different wave-current intensity.

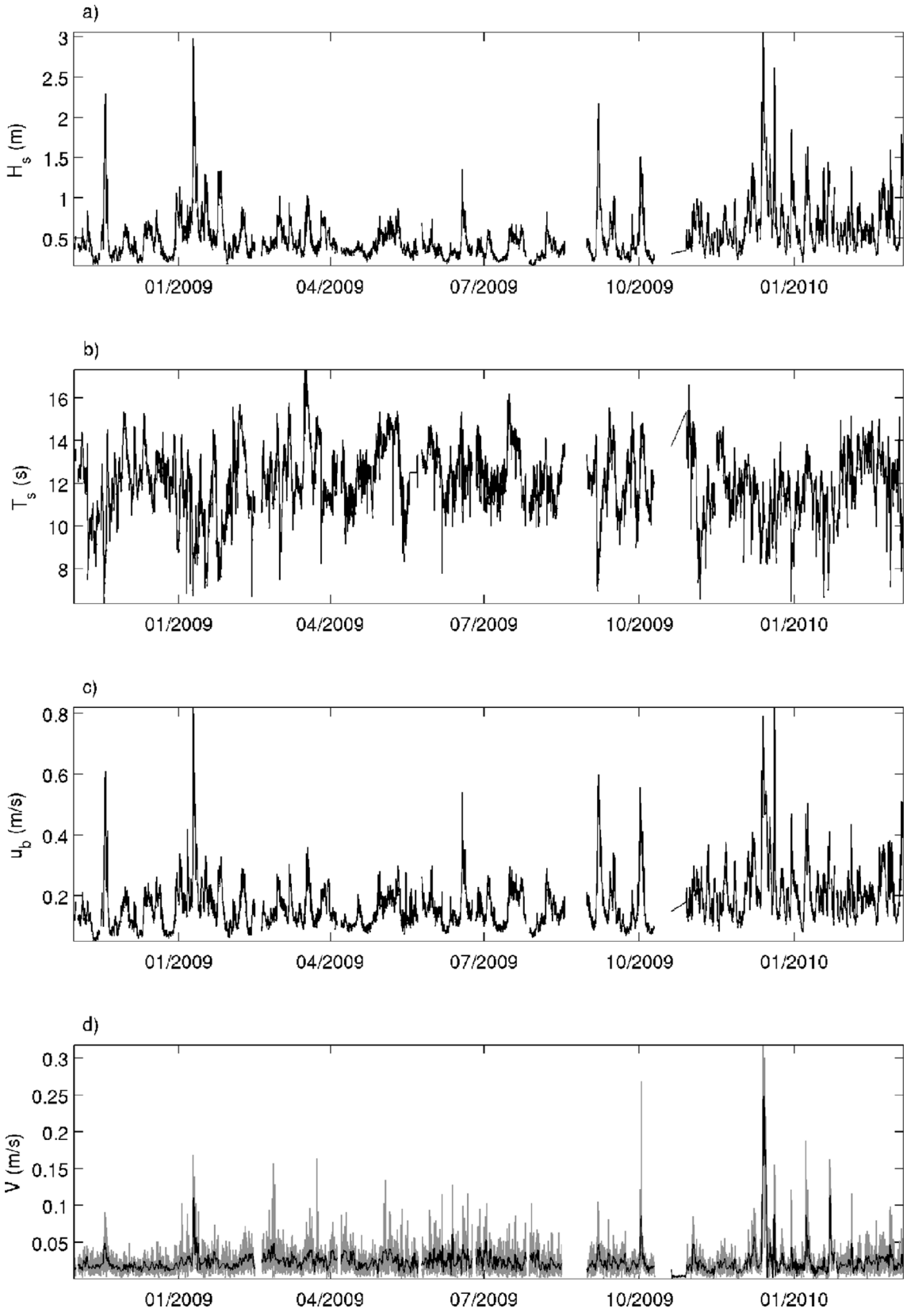

Fig. 11. Time-series of significant wave height (a), wave period (b), bottom orbital velocity (c), and (d) current speed (gray is the raw data; black is the 32-d low-pass filter).

Table 2. Summary statistics for hydrodynamic variables bottom wave orbital velocity u_b, significant wave height H_s, peak wave period T_p and current speed V.

	u_b (m/s)	H_s (m)	T_p (s)	V (m/s)
Mean	0.17	0.	2	0.023
Standard deviation	0.08	0.20	1.65	0.021
Minimum	0.05	0.11	6.36	0.0006
Maximum	0.82	2.16	17.32	0.32

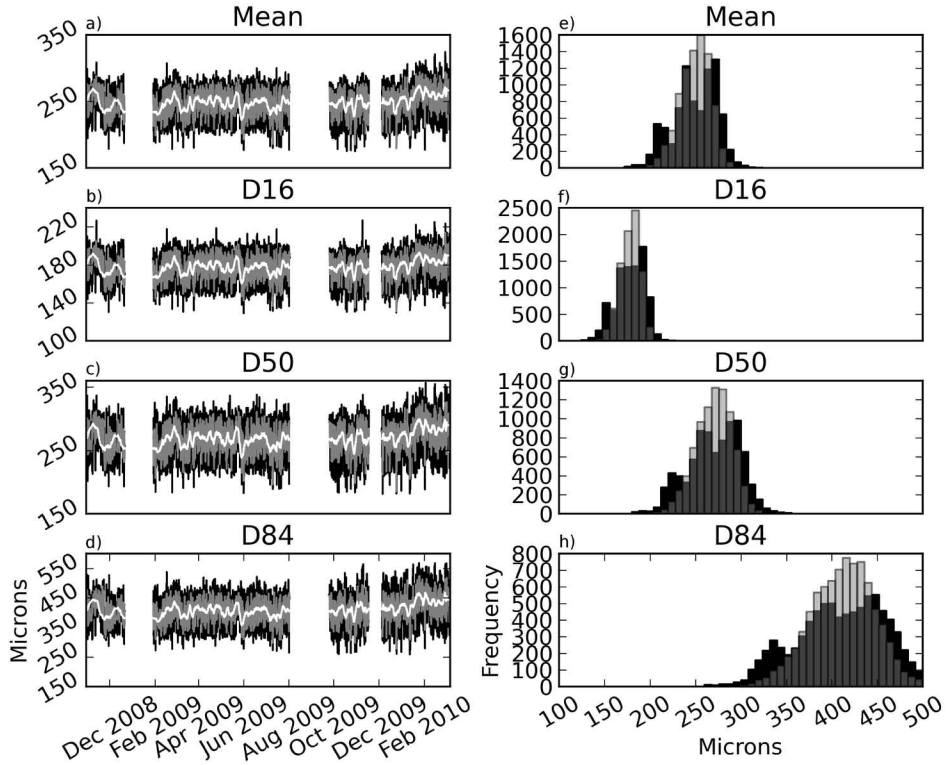

Fig. 12. Left panels: Time-series (Oct 2008–March 2010) of grain-size distribution parameters. In each, black and gray lines are the raw and 6-h running mean, and the white line is a 96 h running mean: (a) mean grain size; (b) 16th percentile; (c) 50th percentile; (d) 84th percentile. Right panels (e through h): distributions of the raw (black, equivalent to the black lines in adjacent panels, a through d); 6 h running mean (dark gray, equivalent to the dark gray lines in adjacent panels) and 96 h running mean (light gray, equivalent to the white lines in adjacent panels).

energetic than the winter of 2008-2009 (mean H_s = 0.4 m). Significant wave height exceeded 1.5 m in Nov 2008, Jan and Feb 2009, Sept 2009, Dec 2009, Jan and March 2010. Mean currents were generally weak (Fig. 11d) except during storm and tsunami events (Lacy et al. 2012) during which they exceeded 0.1 m s^{-1}. Northerly and easterly mean currents were approximately equal magnitude and duration. Current directions were broad-banded with peaks at around 100 and 250° N.

Mean grain size remained around 250 μm for the year preceding first November 2009 (Fig. 12a), with variation around this mean of ± 30% over time-scales of up to 1 week. Median grain size (Fig. 12c) was always slightly coarser than the mean, indicating a distribution skewed toward finer grain sizes. The distributions of each percentile are significantly more Gaussian with a 6-h running mean compared with the (nonfiltered) hourly time-series (Fig. 12e-h). At all times in the record, the variations around the longer-term mean had some temporal structure, in that fluctuations tended to last for several hours up to several days (Fig. 13), which suggests that grain size was responding to time-varying flow conditions. With reference to Table 1, we can effectively rule out camera repositioning (process 1) and onshore/offshore transport (process 8) as processes that might explain this trend because they operate over different time-scales than those observed (hours to days). Changes in grain size distribution shape can help pinpoint the likely cause: examination of the fine (Fig. 12b) and coarse (Fig. 12d) tails of the distribution over short time-scales (up to a few days) suggest short-lived winnowing processes where the fines

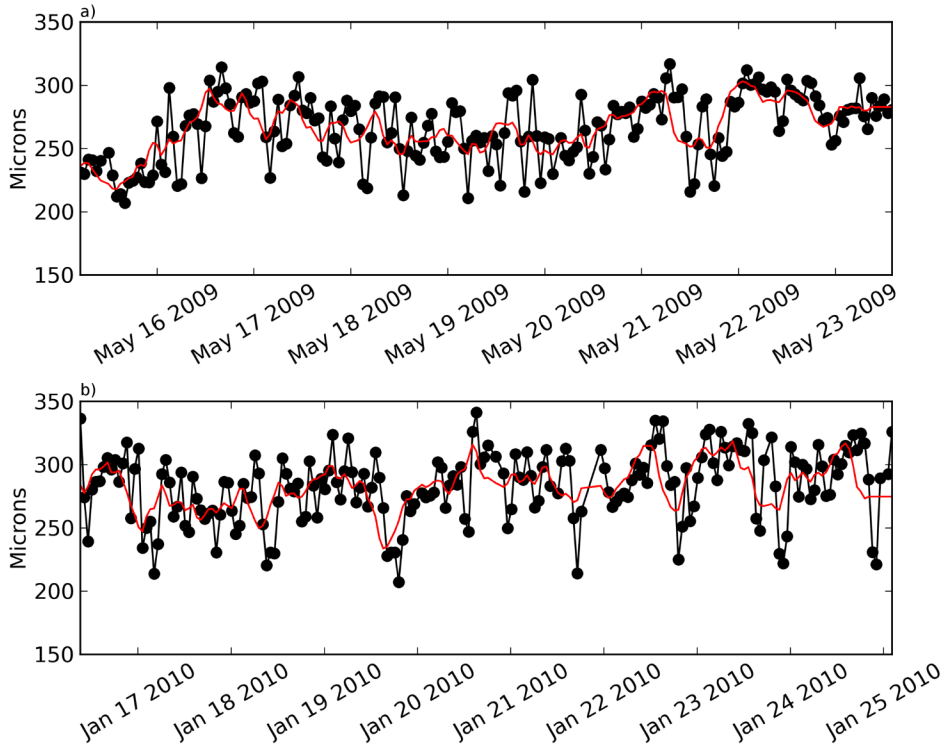

Fig. 13. Two example time-series, drawn at random and each lasting a few days, illustrating typical short-term variability in grain size. In each, the black dots are the hourly samples and the smooth line is the 6 hours running mean. Some coherent structure is evident, and the data are much less spiky than would be expected by a random signal.

were preferentially suspended. The advection of patches of homogeneous sediment past the measurement location due to quasi-periodic pulses of sediment transport would have presumably caused characteristic changes in the mean and standard deviation of grain sizes rather than the observed preferential depletion of fines.

Grain size increased slightly early December 2009 (Fig. 11a), and remained coarser thereafter, with a mean of 275 μm. The measured mean grain sizes were within the same range as sieved grab samples (Fig. 2). Given both the gradual nature of the coarsening, the same camera, camera settings, instrument position, and identical image processing used before and after down-time, we are confident the coarsening was real.

Regional grain-size trends

Data collected from the extended region offshore of Santa Cruz around the hydraulic system location provide an insight into grain-size trends in the vicinity over several hundreds of meters (Fig. 14). A coarsening trend is observed simultaneously in the 10-15 m, 10 m (the depth at which the seafloor observatory was situated), and 5-10 m depth ranges and at the beach during October, November, and December 2009. During late December, the grain size at the seafloor observatory site also coarsened (Fig. 12a). In deeper water (15-20 m), however, the seabed fined until December 2009, when a large increase in grain size was observed.

Discussion

Grain-size variability over time and space

The envelope of variability of grain size at a single point in 10 m water depth was found to be around ± 50 μm (Fig. 12) over almost 18 months, around 40% of the mean of all observations, and which was approximately the same as the variability over the entire nearshore region in just a few months (Fig. 14). The grain size variance at time-scales of days to weeks (up to 30%) was (1) much greater than measurement error at that time-scale (which averaged to << 10%); (2) almost as large as the variance over 18 months (around 40%); and (3) approximately equal to the spatial variability observed over tens of meters.

Long-term variability

In the absence of a change in the sediment supply, or an anomaly in forcing (for example, unusually large storms or tsunamis), the data at the Santa Cruz site suggest not to expect variations in mean sand grain size of greater than approximately 40% over months to years. At the Santa Cruz site, fluvial inputs of fine cohesive sediments in particular would have had the potential to cause the greatest change in grain size (Storlazzi and Jaffe 2002). Unfortunately, this did not occur during the present study, however the physics of entrainment and deposition of non-cohesive and cohesive sediment are

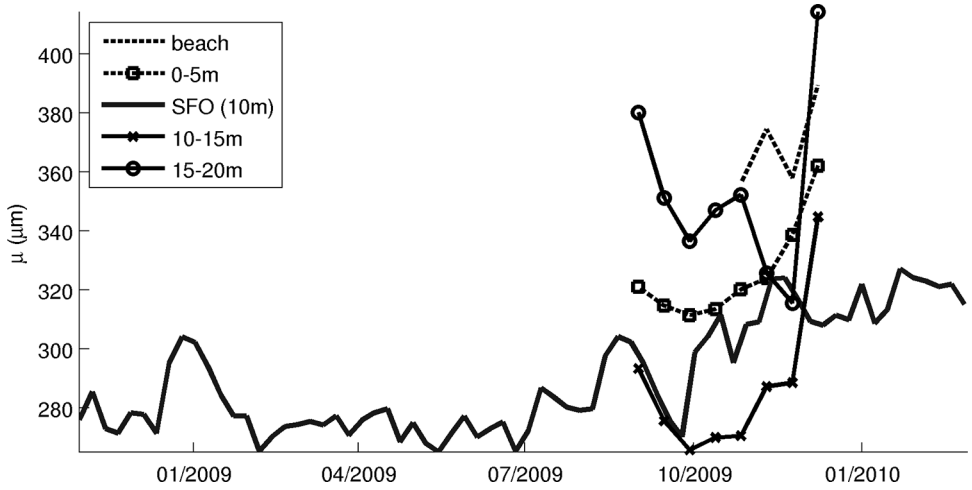

Fig. 14. Time-series of mean grain size (2-weekly averages) at various locations in the nearshore of Santa Cruz. The solid line is the hydraulic camera system in 10 m water depth. The dashed line is the record on the intertidal beach. The squares, crosses, and circles from the 0-5 m, 10-15 m, and 15-20 m depth ranges, respectively, in the vicinity of the study site.

sufficiently different as to enable them to coexist in shelf and nearshore environments, with or without some degree of spatial segregation (Holland and Elmore 2008).

The long-term trend was one of near constant mean grain size for 13 months with random fluctuations of ± 50 μm, followed by 1 month of sustained coarsening associated with more energetic wave conditions, and a further plateau for the remaining 4 months at a larger grain size. The period of sustained coarsening during energetic wave activity could have been due to either preferential winnowing and export of fine grains (item 7 in Table 1), or input of new (coarser) sediment supplies from cross- or along-shelf sediment transport (item 8 in Table 1). Winnowing is consistent with the observed increases in grain size, but is inconsistent with the concurrent increases in sample standard deviations. A new coarser sediment supply is more likely because this would cause both mean and standard deviation of grain size to increases (Table 1), which is what was observed (Fig. 12).

The most likely source of this new, coarser, sediment was probably from further inshore. Previous studies have shown that Santa Cruz beaches and inshore region are composed of coarser material than further offshore, and that these sands are highly mobile primarily due to alongshore currents caused by waves refracting into the Bay, cross shelf currents and strong tidal currents in the eastern part of the Bay (Watt and Greene 2002; Edwards 2002; Storlazzi and Jaffe 2002; Storlazzi et al. 2010). Regional grain size surveys during this time indicate that the entire nearshore region from beach to 15 m water depth was undergoing a similar coarsening, with an apparent lag toward deeper water suggestive of offshore sediment transport (Fig. 13). Accounting for these regional trends in grain size is difficult without sediment-transport or bed-elevation observations at different water depths, but it is postulated that wave energy was sufficient to cause offshore migration of relatively coarse beach sediment. If so, it would conform to the classical model for cyclical changes in beach volumes (Shepard 1950; Sonu and Van Beek 1971), where storm-generated waves cause beach erosion, and sediment accumulates on a winter bar or bank offshore beyond the surf zone.

The above scenario is more likely than the alternative, winnowing of finer-grained surficial sediment and exposure of coarser-grained subsurface material, because the observed change in the grain size distribution was a widening in the coarse tail of the size-distribution rather than a removal of the fine tail. However, it is also possible that some mixing of surface and subsurface material was responsible for some observed changes in grain size.

Comments and recommendations

A remotely operated underwater video microscope system collected an ≈18-month high-frequency record of images of the seabed, in which individual grains were well resolved, on a wave-dominated, predominantly sandy inner continental shelf site. Measurements were insensitive to flow conditions and water clarity (suspended-sediment concentration).

Grain-size distributions were estimated from each image using completely automated methods with a root-mean-squared error of the mean grain size of less than 20%. Photographic surveys carried out by scuba divers in the vicinity of the hydraulic camera system indicated that measurements of grain size were representative of the area. Very high frequency measurements showed that the typical sample frequency of 1 hour was sufficient to capture the observed variance in grain size.

A 1-month period of sustained coarsening was observed, possibly the input of slightly coarser beach sand due to offshore sediment transport from the surf zone onto the inner shelf under energetic waves. This observation was supported by data from regular spatial surveys of grain size during this time.

Grain-size data collected over the entire nearshore suggested that observed mean grain size variability at the instrument location over 18 months was approximately equal to the variation in grain size over the entire nearshore area over a few months. Variability over days to weeks approximated the spatial variability over tens of meters. These results suggest that numerical models of sand transport on the inner shelf should consider variability due to likely mean grain size changes of several tens of percent over timescales of days to months.

In future deployments, the ability to measure both surface and subsurface sediment characteristics at the same frequency and resolution would be a further advance (Blanpain et al. 2009). These subsurface considerations are especially important for fine-grained sediment shelf environments when significant sediment-transport events are highly intermittent, allowing significant amounts of consolidation and bioturbation to occur between events.

High-frequency sampling suggested that the usual hourly sampling scheme was sufficient to capture the mean and standard deviation under low to moderate energy conditions. However, a future system would ideally increase sample frequency during storms when most grain-size changes are expected to occur. A sample frequency of a few minutes might be required to detect bed-sediment changes caused by the passage of small bedforms or bedload sheets and by resuspension due to individual waves or wave groups (Table 1).

Hydrodynamically significant changes in grain size over time-scales up to days might be better elucidated by a combination of (1) more frequent sampling, which would reduce the observed error of individual hourly measurements of up to 20%, according to standard error of the mean, and similarly enhance the likelihood of detecting small changes over short time-scales (a few hours to days), and (2) a sampling scheme that is able to collect a time series of grain-size data from an area, rather than a point, of the seafloor with a spatially randomized sampler system, perhaps similar to that described by Wheatcroft et al. (2007). This latter advance would enable variability due to camera repositioning to be evaluated, as well as provide important information on spatial variability of sediment moving across the seabed.

Acknowledgments

This research was funded by the U.S. Geological Survey Coastal and Marine Geology Program. Any use of trade, product, or firm names is for descriptive purposes only and does not imply endorsement by the U.S. government. Thanks to Josh Logan, Tom Reiss, Jamie Grover, and Pete Dal Ferro (all at USGS Santa Cruz) for diving and boat handling. Thanks to Daniel Conley, Peter Ganderton, and volunteers at the Coastal Processes Research Group at Plymouth University, UK, for help with installing the wave-powered system. Parker Allwardt carried out many manual point-counts on images for method validation. Kevin O'Toole and Tim Elfers provided additional technical support. Theresa Fregoso prepared the map in Fig. 2, and Shandy Buckley assisted with data processing. Thanks to Jon Warrick and two anonymous reviewers for constructive comments, which significantly improved the manuscript.

References

Austin, M. J., and D. Buscombe. 2008. Morphological change and sediment dynamics of the beach step on a macrotidal gravel beach. Mar. Geol. 249:167-183 [doi:10.1016/j.margeo.2007.11.008].

Bailard, J. 1981. An energetics total load sediment transport model for a plane sloping beach. J. Geophys. Res. 86(C11):10938-10954 [doi:10.1029/JC086iC11p10938].

Barnard, P. L., D. M. Rubin, J. Harney, and N. Mustain. 2007. Field test comparison of an autocorrelation technique for determining grain size using a digital 'beachball' camera versus traditional methods. Sed. Geol. 201:180-195 [doi:10.1016/j.sedgeo.2007.05.016].

Blanpain, O., and others. 2009. Dynamic sediment profile imaging system (DySPI): a new field method for the study of dynamic processes at the sediment-water interface. Limnol. Oceanogr. Methods 7:8-20 [doi:10.4319/lom.2009.7.8].

Buscombe, D. 2008. Estimation of grain-size distributions and associated parameters from digital images of sediment. Sed. Geol. 210:1-10 [doi:10.1016/j.sedgeo.2008.06.007].

———. 2013. Transferable wavelet method for grain size-distribution from images of sediment surfaces and thin sections, and other natural granular patterns. Sedimentology 60:1709-1732 [doi:10.1111/sed.12049].

———, and G. Masselink. 2009. Grain-size information from the statistical properties of digital images of sediment. Sedimentology 56:421-438 [doi:10.1111/j.1365-3091.2008.00977.x].

———, and D. M. Rubin. 2012. Advances in the simulation and automated measurement of well sorted granular material. Part 2: Direct measures of particle properties. J. Geophys. Res. 117:F02002.

———, D. M. Rubin, and J. A. Warrick. 2010. A universal approximation to grain size from images of non-cohesive sediment. J. Geophys. Research 115:F02015.

Conley, D. C., S. Falchetti, I. P. Lohmann, and M. Brocchini. 2008. The effects of flow stratification by non-cohesive sediment on transport in high-energy wave-driven flows. J. Fluid Mech. 610:43-67 [doi:10.1017/S0022112008002565].

Cookman, J., and P. Flemings. 2001. STORMSED1.0: hydrodynamics and sediment transport in a 2D, steady-state, wind- and wave-driven coastal circulation model. Comp. Geosci. 27:647-674 [doi:10.1016/S0098-3004(00)00121-7].

Diplas, P., and J. B. Fripp. 1992. Properties of various sediment sampling procedures. J. Hydraul. Eng. 114:484-501 [doi:10.1061/(ASCE)0733-9429(1988)114:5(484)].

Doucette, J. S. 2002. Geometry and grain-size sorting of ripples on low-energy sandy beaches: field observations and model predictions. Sedimentology 49:483-503 [doi:10.1046/j.1365-3091.2002.00456.x].

Edwards, B. 2002. Variations in sediment texture on the northern Monterey Bay Marine Sanctuary continental shelf. Mar. Geol. 181:83-100 [doi:10.1016/S0025-3227(01)00262-6].

Greenwood, B., and R. G. D. Davidson-Arnott. 1972. Textural variations in sub-environments of the shallow water wave zone, Kouchibouguac Bay, New Brunswick. Can. J. Earth Sci. 9:679-688 [doi:10.1139/e72-058].

Harris, C. K., and P. Wiberg. 2002. Across-shelf sediment transport: interactions between suspended sediment and bed sediment. J. Geophys. Res. 107:C1.

Harris, P., and R. Coleman. 1998. Estimating global shelf sediment mobility due to swell waves. Mar. Geol. 150:171-177 [doi:10.1016/S0025-3227(98)00040-1].

Hartley, R., and A. Zisserman. 2003. Multiple view geometry (2nd ed.). Cambridge.

Hay, A. E., and D. Wilson. 1994. Rotary sidescan images of nearshore bedform evolution during a storm. Mar. Geol. 119:57-65 [doi:10.1016/0025-3227(94)90140-6].

Heikkilä, J., and O. Silvén. 2007. A four-step camera calibration procedure with implicit image correction, p. 1106-1112. IEEE Computer Society Conference on Computer Vision and Pattern Recognition (CVPR'97) San Juan, Puerto Rico.

Holland, K. T., and P. A. Elmore. 2008. A review of heterogeneous sediments in coastal environments. Earth Sci. Rev. 89:116-134 [doi:10.1016/j.earscirev.2008.03.003].

Lacy, J., D. Rubin, and D. Buscombe. 2012. Currents, drag and sediment transport induced by a tsunami. J. Geophys. Res. 117:C09028.

Larson, M., and N. Kraus. 1995. Prediction of cross-shore sediment transport at different spatial and temporal scales. Mar. Geol. 126:111-127 [doi:10.1016/0025-3227(95)00068-A].

Madsen, O. 1994. Spectral wave-current bottom boundary layer flows, p. 384-398. *In* Proceedings 24th International Conference on Coastal Engineering, ASCE.

Masselink, G., D. Buscombe, M. J. Austin, T. O'Hare, and P. E. Russell. 2008. Sediment trend models fail to reproduce small-scale sediment transport patterns on an intertidal beach. Sedimentology 55:667-687 [doi:10.1111/j.1365-3091.2007.00917.x].

McFetridge, W., and P. Nielsen. 1985. Sediment suspension by non-breaking waves over rippled beds. Tech. Rep. UFL/COEL-85/008, Coastal and Oceanographical Engineering Department, Univ. of Florida.

Miller, R. L., and J. M. Ziegler. 1958. A model relating dynamics and sediment pattern in equilibrium in the region of shoaling waves, breaker zone, foreshore. J. Geol. 66:417-441 [doi:10.1086/626526].

OpenCV. 2014. Camera calibration with OpenCV. <http://docs.opencv.org/trunk/doc/tutorials/calib3d/camera_calibration/camera_calibration.html>

Ribberink, J., and Z. Chen. 1993. Sediment transport of fine sand under asymmetric oscillatory flow. Tech. Rep. H 840.20, Part VII, WL—Delft Hydraulics, the Netherlands.

Rubin, D. M. 2004. A simple autocorrelation algorithm for determining grain size from digital images of sediment. J. Sed. Res. 74:160-165 [doi:10.1306/052203740160].

———, H. Chezar, J. N. Harney, D. J. Topping, T. S. Melis, and C. R. Sherwood. 2007. Underwater microscope for measuring spatial and temporal changes in bed-sediment grain size. Sed. Geol. 202:402-408 [doi:10.1016/j.sedgeo.2007.03.020].

Scheidegger, A. E., and P. E. Potter. 1967. Bed thickness and grain size: cross-bedding. Sedimentology 8:39-44 [doi:10.1111/j.1365-3091.1967.tb01304.x].

Shepard, F. 1950. Beach cycles in southern California. Tech. rep., Beach Erosion Board, U.S. Army Corps of Engineers.

Sonu, C., and J. Van Beek. 1971. Systematic beach changes on the Outer Banks, North Carolina. J. Geol. 79:416-425 [doi:10.1086/627649].

Storlazzi, C., and B. Jaffe. 2002. Flow and sediment suspension events on the inner shelf of central California. Mar. Geol. 181:195-213 [doi:10.1016/S0025-3227(01)00267-5].

———, and others. 2010. The dynamics of fine-grained sediment dredged from Santa Cruz harbor. USGS Open-File Report 2011-1045.

van der Werf, J., J. Ribberink, T. O'Donoghue, and J. Doucette. 2006. Modelling and measurement of sand transport processes over full-scale ripples in oscillatory flows. Coast. Eng. 53:657-673 [doi:10.1016/j.coastaleng.2006.02.002].

Warrick, J. A., D. M. Rubin, P. Ruggiero, J. N. Harney, A. E. Draut, and D. Buscombe. 2009. Cobble cam: grain-size measurements of sand to boulder from digital photographs and autocorrelation analyses. Earth Surface Proc. Landforms 34:1811-1821 [doi:10.1002/esp.1877].

Watt, S., and H. Greene. 2002. Monitoring dredged upper Santa Cruz Harbor mixed sand and mud sediment released into the nearshore area of Santa Cruz, California. Tech. report. Santa Cruz Harbor Port District and the California Department of Boating and Waterways.

Wheatcroft, R. A., A. W. Stevens, and R. V. Johnson. 2007. In situ time-series measurements of sub-seafloor sediment properties. IEEE J. Ocean. Eng. 32:862-871 [doi:10.1109/JOE.2007.907927].

Wilcock, P. 1988. Methods for estimating the critical shear stress of individual fractions in mixed size sediment. Water Resourc. Res. 24:1127-1135 [doi:10.1029/WR024i007p01127].

Zhang, Y., D. Swift, S. Fan, A. Niedoroda, and C. Reed. 1999. Two-dimensional numerical modeling of storm deposition on the northern California shelf. Mar. Geol. 154:155-167 [doi:10.1016/S0025-3227(98)00110-8].

Submitted 23 November 2013
Revised 27 May 2014
Accepted 6 June 2014